Bio-Design and Manufacturing (2025) 8:442–460
https://doi.org/10.1631/bdm.2400231

RESEARCH ARTICLE

Force-controlled 3D mechanical stretching to enhance the exosome secretion of bone mesenchymal stem cells for bone repair

Jie Wu[1,2,3] · Hao Wang[4] · Tao Sun[5] · Qing Shi[5] · Xie Chen[5] · Yuanbo Qi[1,2,3] · Sheng Tao[1,2,3] · Jiahua Zhao[6] · Daohong Liu[1,2,3]

Received: 11 June 2024 / Accepted: 18 September 2024

Abstract

Exosomes derived from bone mesenchymal stem cells (BMSCs) show promising potential for treating bone defects. However, their clinical application is hindered by low yield and insufficient repair ability. Three-dimensional (3D) mechanical stimulation has been a well-known method for enhancing exosome secretion; however, the traditional stimulation process is always achieved by controlling the displacement of manipulators, which may induce uneven loading distribution and degradation of stimulation strength. Here, we propose a micro-stretching manipulator that automatically controls the stretching force applied to gelatin methacryloyl (GelMA)/hyaluronic acid methacryloyl (HAMA) hybrid hydrogel sheets containing BMSCs within an incubator. To ensure the structural stability of the sheets after long-term stretching, the mixing ratio between GelMA and HAMA was optimized according to the mechanical property response of the sheets to cyclical loading. Subsequently, force-controlled mechanical loading was applied to the BMSC-laden sheets to produce exosomes. Compared with displacement control, force-controlled loading provides a more stable force stimulation, thereby enhancing exosome secretion. Furthermore, continuously stimulated exosomes exhibited a stronger capacity for promoting osteogenic differentiation of BMSCs and facilitating the repair of bone defects in a rat model. These findings suggest that force-controlled loading of cell-laden hydrogels offers a novel approach for the production of BMSC-derived exosomes and their application in bone repair.

Jie Wu and Hao Wang have contributed equally to this work.

✉ Jiahua Zhao
jiahua301@163.com

✉ Daohong Liu
domb@vip.sina.com

[1] Department of Orthopedics, The First Medical Center of Chinese PLA General Hospital, Beijing 100853, China

[2] Senior Department of Orthopedics, The Fourth Medical Center of Chinese PLA General Hospital, Beijing 100142, China

[3] Department of Orthopedics, The Eighth Medical Center of Chinese PLA General Hospital, Beijing 100091, China

[4] Department of Orthopaedics, Lanzhou University Second Hospital, Lanzhou 730030, China

[5] Intelligent Robotics Institute, School of Mechatronical Engineering, Beijing Institute of Technology, Beijing 100081, China

[6] Department of Thoracic Surgery, The Sixth Medical Center of Chinese PLA General Hospital, Beijing 100048, China

Graphical abstract

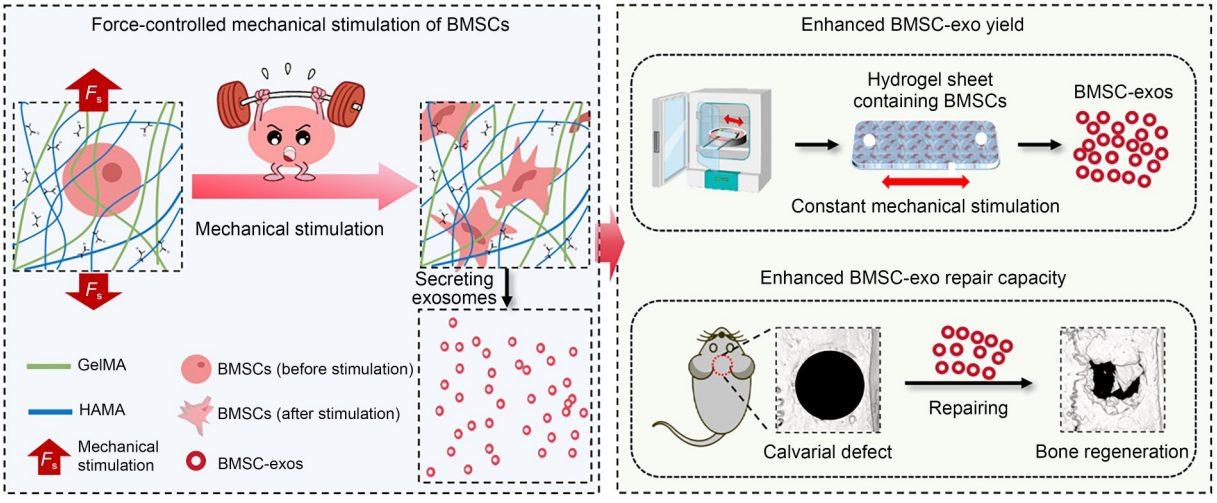

Keywords Exosomes · Force control · Mechanical loading · Mesenchymal stem cells · Bone repair

1 Introduction

Large bone defects that result from trauma, infection, tumors, and other etiologies pose a prevalent and challenging clinical issue [1, 2]. The traditional method of using autogenous bone grafts for filling has several limitations, such as limited bone volume and complications at the donor site [3]. Although artificial bone repair materials are an important resource for repairing bone defects, they lack biological activity and osteoinductivity [4, 5]. Bone mesenchymal stem cells (BMSCs) have become important seed cells in the field of tissue engineering because of their capability for self-renewal, multidifferentiation, and paracrine activity [6]. In a study of the application of BMSCs in tissue engineering, several limitations were identified, including low survival rates after transplantation, tumorigenicity, and immunogenicity [7]. Recent studies have revealed that BMSC-derived exosomes (BMSC-exos) perform most of the functions of BMSCs. Furthermore, they exhibit no immunogenicity or risk of tumor formation and offer the advantages of targeting, ease of use, and processability. Furthermore, BMSC-exos play a crucial role in treating bone-related diseases by maintaining bone metabolism homeostasis, modulating bone innervation, regulating immunity, and promoting vascularization [8, 9]. Low yield presents a significant obstacle to the engineering application of exosomes [10, 11]. Studies have indicated that exosome production can be enhanced by appropriate physicochemical stimuli [11]. Given the challenges in ensuring the biological safety of various biochemical stimuli, there has been a growing focus on physical stimulation programs. Wang et al. [12] found that the secretion of exosomes from periodontal ligament cells increased 30 times under cyclic stretching conditions compared with that under static culture conditions. Mechanical stimulation plays an important role in the proliferation, differentiation, and paracrine of BMSCs. Therefore, achieving higher BMSC-exos production is theoretically possible with appropriate mechanical stimulation. Meanwhile, the insufficient repair ability poses another challenge for the clinical application of exosomes [8]. Mullen et al. [13] found that mechanical stretch stimulation can enhance the ability of exosomes to promote cell proliferation and myogenic differentiation by changing the composition of miRNAs contained in exosomes. Xiao et al. [14] found that BMSC-exos, following cyclic stretch treatment, can inhibit osteoclast generation by attenuating the activity of the NF-κB signaling pathway. Furthermore, mechanical stimulation-induced BMSC-exos exhibited superior ability in inhibiting osteoporosis. Therefore, increasing the production and enhancing the function of exosomes through mechanical stimulation help realize the clinical application of exosomes; however, there is still a lack of effective methods for achieving this goal.

Current research on the effects of mechanical stimulation on mesenchymal stem cell (MSC) differentiation and paracrine activity primarily focuses on two-dimensional (2D) culture environments [13, 15]; however, some studies have demonstrated that the responses of cells to various stimuli in a three-dimensional (3D) culture environment, which is more similar to the physiological state, are inconsistent with or even contrary to those in 2D culture [16–19]. Therefore,

investigating the effect of mechanical stimulation on the secretion and function of BMSC-exos in a 3D culture environment is necessary. Recently, a novel magnetically stretched cell-laden collagen hydrogel was developed to show the enhanced osteogenic activity of MSC-derived exosomes in the 3D space [20]. However, traditional mechanical loading methods for 3D-cultured cells are mostly based on elastic membrane platforms [21, 22]. The expansion of the membrane allows for the straining of cell-laden hydrogels installed on the membrane; however, the resulting mechanical loading varies depending on the location of the cells encapsulated in the hydrogel [22]. In contrast, a stretching apparatus can use mechanical grippers to stretch cell-laden hydrogels for mechanical loading. A uniform tensile force can then be applied along the stretched direction of the hydrogel [23]. Most current 3D mechanical loading methods are based on hydrogel deformation, with the degree of deformation being controlled by the displacement of the membrane and grippers [21, 22, 24]. However, the mechanical properties of hydrogels can gradually weaken under displacement-controlled loading modes. Consequently, the mechanical force applied on cells due to hydrogel deformation may be attenuated accordingly. The maintenance of sustained force stimulation during long-term dynamic culture remains challenging, potentially hindering the consistent attainment of a high yield of functionally enhanced exosomes. Therefore, adopting a mechanical loading model based on force control is necessary to further explore the effect of unattenuated force stimulation on the production and osteoinductive ability of BMSC-exos.

In this study, we developed a force-controlled mechanical loading method to facilitate the production of BMSC-exos under long-term and constant force stimulation in the 3D space. The schematic of the entire method is shown in Fig. 1. BMSCs were encapsulated into a gelatin methacryloyl (GelMA)/hyaluronic acid methacryloyl (HAMA) hybrid sheet for 3D culture. A force-controlled loading instrument was developed to dynamically stretch the sheet in an incubator environment. The optimal GelMA/HAMA ratio was determined based on the response of the sheet's mechanical properties to dynamic stretching. Subsequently, force-controlled mechanical loading was applied to the BMSC-laden sheet for a 7-d cell culture period. Based on this culture method, we investigated the impact of constant force stimulation on the amount of exosome secretion and its contribution to osteogenesis. The subsequent application in repairing rat bone defects further demonstrated that the combination of optimized 3D culture sheets and force-controlled stimulation can provide an effective method for the application of BMSC-exos in the field of bone regeneration.

2 Methods

2.1 Cell culture and characterization of BMSCs

Sprague–Dawley rat BMSCs were obtained from OriCell Biosciences Co., Ltd (Guangzhou, China). The expression of BMSC surface markers, including CD34 (Invitrogen Biotech

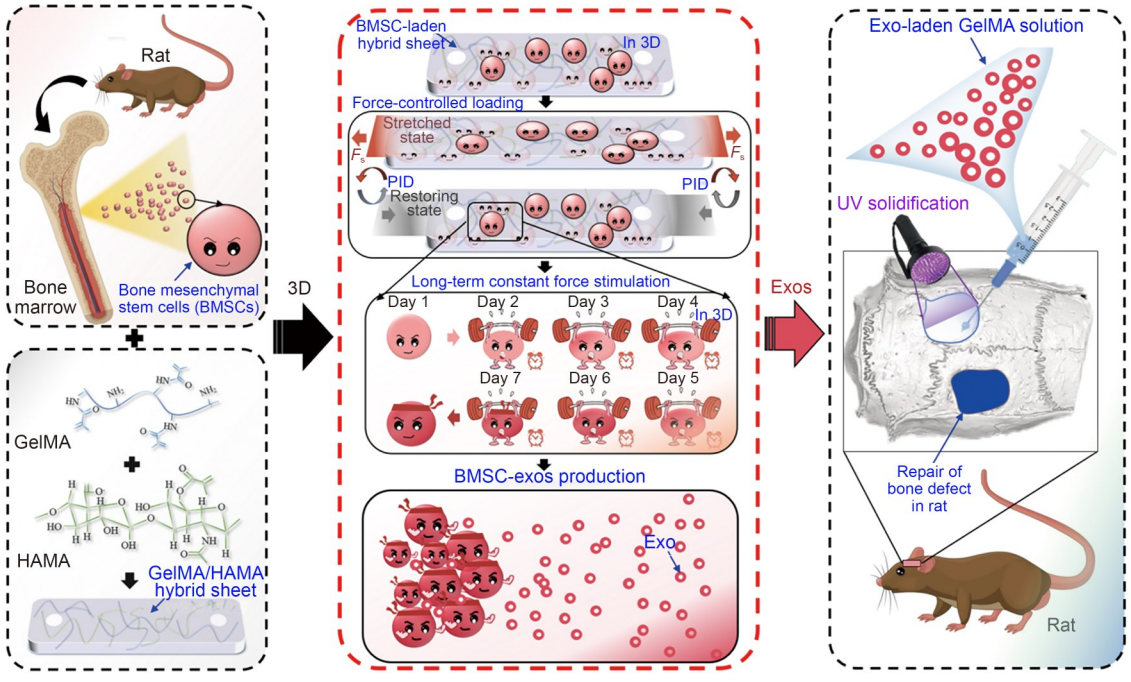

Fig. 1 Schematic of long-term force-controlled 3D mechanical stimulation to produce exosomes derived from BMSCs for repairing bone defects. UV: ultraviolet

Co., Ltd., California, USA), CD45 (BioLegend Biotech Co., Ltd., California, USA), CD90 (BioLegend Biotech Co. Ltd.), and CD105 (Invitrogen Biotech Co., Ltd.), was analyzed using flow cytometry and FlowJo 10.0. According to the manufacturer's instructions, BMSCs were cultured in osteogenic, adipogenic, and chondrogenic induction media (OriCellBio RAXMX-90021, RAXMX-90031, and RAXMX-90041, respectively) and stained with alizarin red (OriCellBio, ALIR-10001), oil red O, and alcian blue, respectively, to assess their differentiation ability.

2.2 3D culture of BMSCs

For the 3D culture, we used GelMA (EFL-GM-30) and HAMA (EFL-HAMA-150K) provided by Yongqinquan Intelligent Equipment Co., Ltd. (Suzhou, China). The composite hydrogel was prepared using the following concentrations: 5% (50 mg/mL) GelMA (G5 group), 5% GelMA+ 0.1% (1 mg/mL) HAMA (G5H01 group), 5% GelMA+0.3% (3 mg/mL) HAMA (G5H03 group), and 5% GelMA+0.5% (5 mg/mL) HAMA (G5H05 group). The composite hydrogel was then dissolved by immersion in phosphate-buffered saline (PBS) containing the photo-initiator lithium phenyl-2, 4, 6-trimethylbenzoylphosphinate (LAP) (0.25% (2.5 mg/mL)), accompanied by shaking. After filtering the composite hydrogel through a 0.22-μm filter, BMSCs were resuspended in the hydrogel at a cell density of approximately 1.0×10^6 mL^{-1}.

The 3D culture of BMSCs was performed using a hydrogel sheet. To fabricate hydrogel sheets compatible with our loading device, we used a template casting technique. This process began with the creation of an acrylic template featuring a concave structure, which was achieved via computer numerical control (CNC) machining. Subsequently, a polydimethylsiloxane (PDMS) mixture was poured into this template at a 1:10 ratio. Following a heating period of 4 h at 60 °C, the PDMS mold was successfully formed. We then injected 140 μL of cell-laden hydrogel into this mold and cured it using ultraviolet light. Because of the hydrophobic nature of PDMS, the hydrogel sheet could be easily removed from the template for further procedures. The cell-laden hydrogel sheet was then placed in a dish, and the complete medium was added before incubating it in an incubator.

2.3 Mechanical loading instrument

The mechanical loading instrument employed a two-probe configuration for stretching hydrogels, as shown in Fig. S1 (supplementary information). One of the probes, mounted on a linear actuator with a repeatability of ±0.2 μm, was the moving probe and was made of quartz (outer diameter: 1 mm; inner diameter: 0.6 mm). The other probe, mounted on a stepper motor (Newport, California, USA) with a minimum incremental movement of 0.2 μm, was the sensing probe and was also made of quartz (outer diameter: 0.7 mm; inner diameter: 0.5 mm). The deflection of the probe was captured using a digital camera (Supereyes, Shenzhen, China) operating at a frame rate of 15 Hz. Subsequently, using Python script (version 3.8), the deformation-related stretching force F_S was calculated and controlled through an in-house developed program. To ensure stability in culture conditions during stimulation, the probes and hydrogel were enclosed within a transparent operating chamber fabricated using 3D printing technology while being placed inside an incubator (Benchmark, Arizona, USA). Details of the experimental procedures are presented in the supplementary information (Sections S1.1 and S1.2).

2.4 Mechanical stimulation loading protocol

The hydrogel sheets, with or without BMSCs, were precultured for 24 h before being subjected to stretching mechanical stimulation. The loading parameters for displacement control loading (MD group) were set to maintain a displacement control at 10% strain and a frequency of 1 Hz. In the force control group (MF group), force control was applied at the predicted F_S intensity (10% strain) with a frequency of 1 Hz. The static culture (M0 group) was used as the control group. All cultures, whether static or mechanically loaded, were placed in an incubator for cultivation and collected for analysis at the appropriate time points.

2.5 Cell counting kit (CCK)-8 assay and live/dead viability assay

A CCK-8 kit (Dojindo Biotech Co., Ltd., Nagasaki City, Japan) was used to evaluate cell proliferation within various composite hydrogels. On Days 1, 4, and 7 of cell culture, the original medium was replaced with a complete medium containing 10% CCK-8. Following a 2-h incubation in darkness, the medium was transferred to a 96-well plate. Absorbance at 450 nm was measured using an enzyme labeler. Each experimental condition was replicated across five wells, and the entire experiment was performed five times to ensure reliability.

The viability of BMSCs in different composite hydrogels was assessed using a live/dead staining kit (Abbkine Biotech Co., Ltd., Wuhan, China). After 7 d of culture, the hydrogels containing cells were washed three times with PBS. Subsequently, LiveDye/NucleiDye reagent, as recommended in the instructions, was added to each well. Following a 30-min incubation, the culture plates were washed again and examined under a fluorescence microscope (Nikon, Tokyo, Japan).

To further investigate the impact of mechanical stimulation on the proliferation and viability of 3D-cultured BMSCs, we exposed the cells to various mechanical stimuli. On

Days 1, 4, and 7 of mechanical loading, the cell-laden hydrogel sheets of the M0, MD, and MF groups were transferred to a 48-well plate, and CCK8 assay and live/dead staining experiments were performed following the aforementioned steps.

2.6 Cytoskeleton staining

To investigate the impact of mechanical stimulation on the morphology of BMSCs, fluorescein isothiocyanate (FITC)-labeled phalloidin (Solarbio Biotech Co., Ltd., Beijing, China) and 4′,6-diamidino-2-phenylindole (DAPI) (Solarbio Biotech Co., Ltd.) staining solution were used for cytoskeletal and nuclear staining, respectively. On Day 7 of cell culture, the medium in the wells was aspirated and washed three times with PBS. Fixation was then performed using 4% paraformaldehyde for 30 min at room temperature, followed by permeabilization using 0.5% Triton X-100 (Solarbio Biotech Co., Ltd.) for 15 min. The cytoskeleton was then stained with FITC-labeled phalloidin at the recommended concentration and incubated for 12 h at 4 °C in the dark before being rinsed twice with PBS. Nuclei were stained with DAPI solution for 10 min, followed by another wash with PBS before observation under a laser confocal microscope (Nikon).

2.7 RNA-sequencing analysis

To further investigate the effect of mechanical stimulation on BMSCs, mRNA sequencing analysis was performed in cells from the M0 and MF groups. Total RNA was extracted from the samples using TRIzol reagent (Tiangen Biotech Co., Ltd., Beijing, China). The RNA was then assessed and quantified. Subsequently, RNA libraries were developed and sequenced by a commercial sequencing company using Illumina NovaSeq^{TM} 6000. Sequencing data were filtered using Fastp (v0.14.0). The clean reads were then aligned to the reference genome and mapped with the reference coding gene set using HISAT2 (v2.2.0). Subsequently, StringTie (v2.2.1) was used to calculate gene expression levels. Differential expression analysis was performed using Limma (v3.32.10), with the criteria for selecting differentially expressed genes (DEGs) being $|\log_2 FC| \geqslant 1$ and p-value$\leqslant 0.05$. Gene Ontology (GO) and Kyoto Encyclopedia of Genes and Genomes (KEGG) enrichment analyses of DEGs were performed using the R package clusterProfiler. Each group comprised three biological replicates.

2.8 Extraction, identification, and concentration analysis of exosomes

After 7 d of mechanical stimulation, the medium was replaced with an exosome-depleted medium, and the culture was continued for an additional 48 h. The supernatant was collected, and cellular debris was removed via centrifugation at 300g for 10 min, followed by centrifugation at 2000g for 20 min. Subsequently, the supernatant was centrifuged at 10 000g for 30 min and then filtered using a filter with a pore size of 0.22 μm, followed by ultracentrifugation at 100 000g for 70 min. Finally, the supernatant was washed with large volumes of PBS and subjected to another round of centrifugation at 100 000g for an additional period of 70 min. All procedures were performed at 4 °C. The prepared exosomes were resuspended in PBS and stored at −80 °C.

The morphology of the exosomes was observed using a transmission electron microscope (Hitachi, Tokyo, Japan). Western blotting was performed to identify exosome-specific surface markers (i.e., CD9, CD81, TSG101, and Calnexin). Exosomes were lysed using a radio immunoprecipitation assay (RIPA) (Solarbio Biotech Co., Ltd.). Protein samples were normalized and denatured at 95 °C with sodium dodecyl sulfate-polyacrylamide gel electrophoresis (SDS-PAGE) loading buffer (Beyotime Biotech Co., Ltd., Shanghai, China) for 5 min. Subsequently, the proteins were separated using a 4% – 20% Bis-Tris SDS-PAGE gel and transferred onto polyvinylidene fluoride membranes (Bio-Rad, California, USA). The membranes were blocked with EveryBlot Blocking Buffer (Bio-Rad) for 10 min at room temperature and then incubated with primary antibodies overnight. The membranes were then washed three times with Tris-buffered saline Tween (TBST) for 10 min each and incubated with the corresponding secondary antibodies. After another three washes with TBST for 10 min each, Clarity Western ECL Substrate was applied, and images were captured using a G: BOX Chemi XX6 gel doc system (Syngene, Cambridge, UK). Finally, the images were further processed using ImageJ (version 1.8.0). The size and concentration of BMSC-exos were measured using nanoparticle tracking analysis (NTA) software using a NanoSight NS500 instrument (Malvern Instruments, Malvern, UK). To account for variations in the number of cells between different groups, the total number of BMSC-exos was normalized by dividing it by the number of BMSCs to calculate the average number of exosomes secreted per BMSC [25].

2.9 Cellular uptake of exosomes

BMSCs were seeded into eight-well chamber slides at a density of 1.5×10^4 cells/well and cultured overnight in an incubator. BMSC-exos collected from the M0, MD, and MF groups were labeled using an exosome membrane labeling kit (Dojindo Biotech Co., Ltd.) following the manufacturer's instructions. The labeled BMSC-exos were then resuspended in an exosome-free complete medium to a concentration of 1.5×10^8 particles/mL. Subsequently, 300 μL of the medium containing labeled exosomes was added to each well and incubated in the dark for 12 h. After washing three times with

PBS, the cells were fixed, permeabilized, and stained with FITC-labeled phalloidin for the cytoskeleton and DAPI for the nucleus. The stained cells were observed under a confocal laser microscope (Nikon).

2.10 Quantitative reverse transcription polymerase chain reaction (qRT-PCR) analysis

BMSCs were cultured in a 3D environment using the exosome-free complete medium. The control group received the addition of 10% PBS, whereas the M0, MD, and MF groups received the addition of 10% BMSC-exos (1×10^9 particles/mL) extracted from their respective groups (M0, MD, and MF). The positive control group, named as the CI group, was chemically induced with osteogenic induction medium. The expression of osteoblast-related genes in BMSCs from the control, M0, MD, MF, and CI groups was evaluated using qRT-PCR. On Days 7 and 14 of culture, cell-laden hydrogel sheets from the various treatment groups were harvested. The hydrogels were lysed using lysates (Yongqinquan Intelligent Equipment Co., Ltd.) according to the provided instructions. Total RNA was extracted from BMSCs following the guidelines for the TRIzol reagent. Reverse transcription to cDNA was performed using the HiScript III 1st Strand cDNA Synthesis Kit (Nuoweizan Biotech Co., Ltd., Nanjing, China) with gDNA Eraser, strictly adhering to the kit's protocol. qRT-PCR was performed on a real-time PCR system (Applied Biosystems, California, USA) using Universal SYBR Green Supermix (CoWin Biotech Co., Ltd., Boston, USA). The primers used are listed in Table S1 (supplementary information), with Glyceraldehyde-3-phosphate dehydrogenase (GAPDH) serving as the normalization control. Each sample was tested in triplicate, and the experiment was replicated three times. Data were analyzed using the $2^{-\Delta\Delta C_T}$ method.

2.11 Alkaline phosphatase (ALP) and alizarin red staining

ALP staining and alizarin red staining were used to detect the ability of BMSC-exos to promote osteogenic differentiation of BMSCs in the 3D space. According to different treatment methods, the samples were divided into the control, M0, MD, MF, and CI groups. On Day 7 of culture, cell-laden hydrogel sheets were washed with PBS and fixed with 4% paraformaldehyde at room temperature for 20 min. After washing again, the 5-bromo-4-chloro-3-indolyl-phosphate/nitro blue tetrazolium (BCIP/NBT) kit (Beyotime Biotech Co., Ltd.) was applied for ALP staining. After incubation for 2 h at room temperature in the dark, the cells were washed again and observed using a stereomicroscope (Nikon). On Day 14 of culture, the cells were washed and fixed according to the aforementioned steps. The cells were then stained with alizarin red, incubated at room temperature for 5 min, washed again, and observed using a stereomicroscope. ImageJ was used to calculate the area of the positive region.

2.12 Animal experiments

A rat calvarial defect model was used to assess the osteogenic potential of BMSC-exos under various treatment conditions in vivo. Twenty male Sprague–Dawley rats (350–400 g, aged 10–12 weeks) were obtained from SPF Biotechnology Co., Ltd. (Beijing, China). The animals were housed in the animal laboratory of the PLA General Hospital under a 12-h dark/light cycle with ad libitum access to food and water. According to the different treatments, the animals were divided into four groups: the Defect group (bone defect area left empty without implantation), M0 group, MD group, and MF group (bone defect area was implanted with a hydrogel containing BMSC-exos from the M0, MD, and MF groups, respectively). Isoflurane inhalation anesthesia was used. After successful anesthesia, the hair from the eye to the back end of the skull was shaved, the area was disinfected with sterile towels and 75% alcohol, and a 2-cm longitudinal incision was made along the midline of the skull. The skin, subcutaneous tissue, and fascia were cut one by one to expose the skull. A dental trephine was used to carefully drill two full-thickness bone defects approximately 5 mm in diameter into the parietal bone on both sides of the midline of the skull. According to a literature report, the degradation time of GelMA-60 (EFL-GM-60) at a concentration of 10% (0.1 g/mL) in vivo is approximately one month [26]. In this study, GelMA-60 was used as a carrier to sustain the activity of BMSC-exos in the bone defect area. To assess the variance in the bone repair capability of BMSC-exos obtained through different pretreatments, 20 μL of hydrogels containing BMSC-exos with various pretreatments (1.0×10^8 particles/mL) was injected into the bone defect area. Subsequently, the hydrogel was photocrosslinked and cured. The incisions were sutured layer by layer. After awakening from anesthesia, the rats were transferred to a clean cage for independent feeding and provided free access to food and water. Finally, 100 000 U of penicillin sodium was injected intramuscularly for three consecutive days after surgery to prevent infection.

2.13 Micro-computed tomography (CT)

On the eighth postoperative week, the rats were anesthetized with isoflurane inhalation and euthanized. Subsequently, the skulls were dissected and fixed in 4% paraformaldehyde. The skull specimens were scanned using a micro-CT system (Bruker, Karlsruhe, Germany) with a scanning voltage of 70 kV, current of 200 μA, resolution of 6.5 μm, and exposure time of 350 ms. The original images were reconstructed

using NRecon (Bruker) for 3D visualization. CTAnalyzer (Bruker) was used to analyze the region of interest. Parameters such as total volume (TV), bone volume (BV), volume ratio (BV/TV), trabecular number, trabecular thickness, and structure model index were calculated using the software.

2.14 Histological staining

After conducting micro-CT analysis, the skull specimens from each group were decalcified in a 10% ethylenediaminetetraacetic acid solution, embedded in paraffin, and sectioned at 5 μm. The sections underwent hematoxylin–eosin (HE) and Masson staining and were observed using optical microscopy (Leica, Aperio GT450).

2.15 Statistical analysis

GraphPad Prism 9.0 (California, USA) was used for data plotting and statistical analyses. All values are presented as mean±standard deviation. One-way analysis of variance was performed to compare multiple groups, followed by Tukey's post hoc test to compare between different groups. An unpaired two-tailed Student's *t*-test was performed to compare two groups, with a significance level of $p<0.05$.

3 Results

3.1 Stretching culture instrument for force-controlled strain application on sheets

The implementation of mechanical loading on the sheets was facilitated using a stretching culture instrument with the capacity of real-time stretching force control. As illustrated in Figs. 2a and 2b, the instrument comprised a two-probe actuator and a microscope camera, both of which could run steadily in an incubator environment (37 °C, 5% CO_2). The two-probe actuator comprised a sensing probe and an

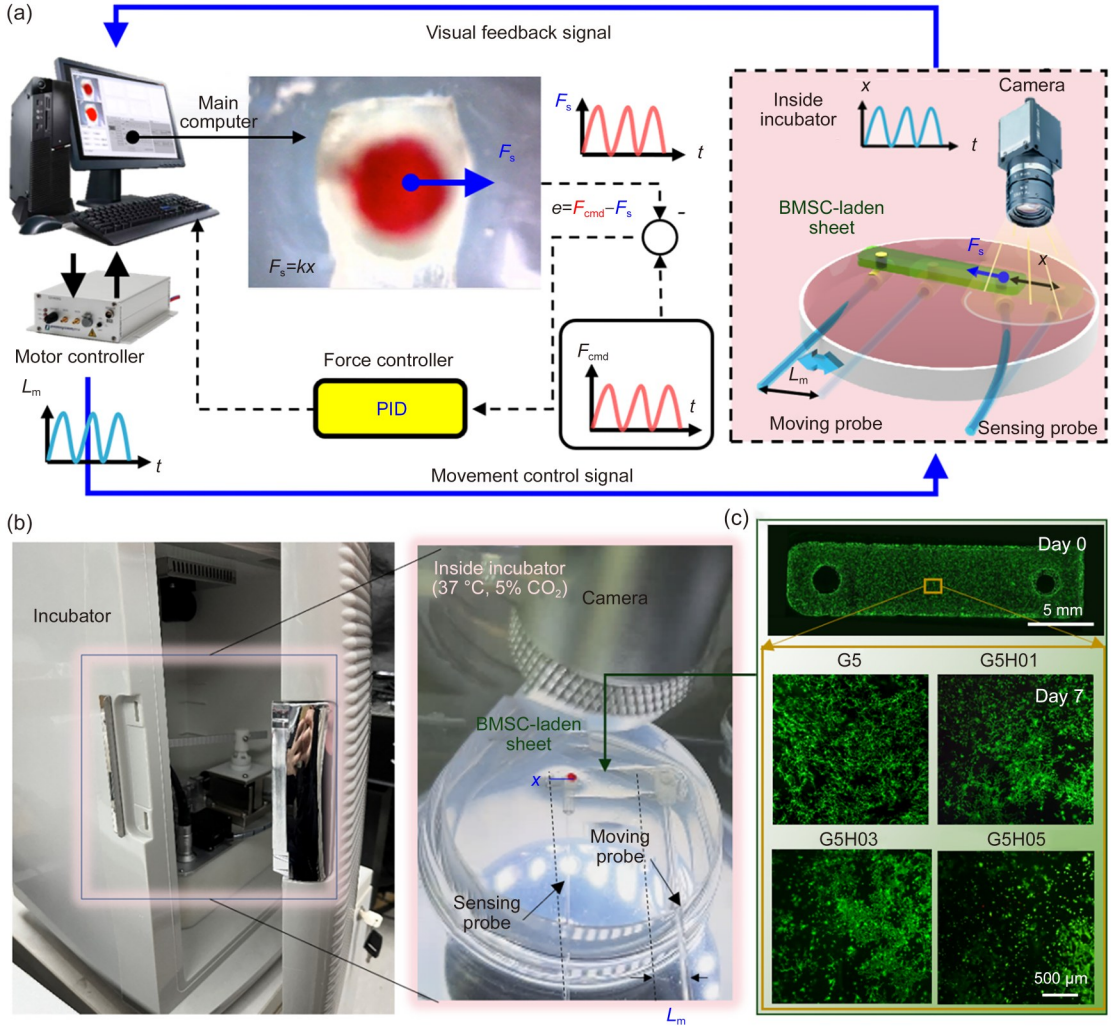

Fig. 2 Force-controlled mechanical loading system. (a) Schematic of the stretching culture instrument with the capacity of real-time stretching force control. (b) Physical picture of the instrument in an incubator. (c) Rectangular GelMA/HAMA hydrogel sheets for 3D BMSC culture

actuating probe, which were horizontally positioned above the culture medium surface of the Petri dish. Two microposts installed on the front ends of the two probes were inserted into the two mounting holes, respectively, in the sheet. When the actuating probe moved away from the sensing probe, the sheet was stretched along its long axis. Stretching force F_s was uniformly delivered from the end of the sheet fixed at the actuating probe to the other end fixed at the sensing probe. The sensing probe then generated a flexing deformation x that could be recorded by the camera mounted above the probe to calculate F_s. To achieve control of F_s during stretching, the system computed the deviation e between the measured F_s and the expected force F_{cmd} in real time and fed it into the proportional-integral-derivative (PID) controller. The output value from the PID controller was then transmitted from the personal computer (PC) to the motor controller to regulate the moving distance L_m of the actuating probe. Such a control method allowed the F_s to constantly match the F_{cmd} in long-term cell culture. Furthermore, the cyclical stretching process in an incubator is shown in Video S1 (supplementary information).

We used 5% GelMA and 5% GelMA mixed with 0.1%, 0.3%, and 0.5% HAMA to form four groups (G5, G5H01, G5H03, and G5H05, respectively) for the fabrication of rectangular hydrogel sheets. The experimental results revealed that the four groups of sheets could be easily fabricated using the traditional PDMS template method (Fig. S2 in the supplementary information). The morphology of the resulting sheets is shown in Fig. 2c; two mounting holes at both ends of the sheets were created for subsequent mechanical loading. The BMSCs used in this study had trilineage differentiation ability and expressed MSC surface markers (Fig. S3 in the supplementary information). Furthermore, BMSCs were embedded in the four sheets at a density of 1.0×10^6 cells/mL, forming a 3D culture environment. Seven-day static cell culture experiments were performed, and the CCK-8 results (Fig. S4 in the supplementary information) showed that the G5 group exhibited the most rapid cell proliferation among all groups. Furthermore, a noticeable decrease in the cell proliferation rate was observed with increasing concentrations of HAMA. Live/dead staining results (Fig. 2c) revealed that the cell viability in all groups exceeded 95%, suggesting that the resulting sheets did not exhibit pronounced cytotoxicity. Furthermore, to apply mechanical stimulation to BMSCs encapsulated in the sheets, the sheets were cyclically strained along their long axis using two stretching methods. The first method was displacement-controlled strain during each loading cycle, in which the stretched distance of the sheets was kept constant, regardless of the change in the internal stress σ in the sheets. The second method was force-controlled strain during each loading cycle, in which a constant stretching force was maintained through the entire sheet without consideration of dimensional changes in the sheet.

3.2 Response of sheets to force-controlled strain application

We performed a simulation using COMSOL to evaluate the effect of these two loading methods on σ in the sheets when stretched to 10% amplitude, as depicted in Fig. 3a and Video S2 (supplementary information). The behavior of the sheets was modeled using a viscoelastic model. It is generally observed that when the loading time t surpasses three times the time constant (3τ), the creep or stress relaxation of the viscoelastic material approaches a stable state. Accordingly, we simulated and analyzed the stress σ distribution from t=0 to t=3τ under force- and displacement-controlled loading. The simulation results showed that the maximum stress in the hydrogel sheet, regardless of the control method, occurred at the micropillar contact point, whereas the strain in the central region remained almost uniform. However, the hydrogel sheet moved a greater distance (Δ) under force-controlled loading than under displacement-controlled loading. Further extracting σ inside the hydrogel sheet along the A–B line for comparison, it was observed that σ started to rise from point A and remained basically constant at the position 2 mm away from point A, after which σ started to fall from the position 2 mm away from point B until point B was close to 0. When the force was controlled, looking at the part marked by the dotted line in the middle part of the $A-B$ line, σ remained almost constant from $t=\tau$ to t=3τ. However, without force control, σ decreased at first from $t=\tau$ to t=2τ but remained unchanged from 2τ to 3τ, indicating that after stress relaxation, the hydrogel sheet tended to be stable. The simulation results revealed that compared with displacement-controlled loading, force-controlled loading could effectively prevent stress decay to provide more stable force stimulation during the entire cell culture process.

Furthermore, cell-free sheets in the four groups were cyclically strained using the proposed system, and the real-time changes in F_s and the sheet strain ε were recorded to analyze the response of the sheets to the two stretching methods. Before testing, we first determined the magnitude of F_s when the four sheets were statically stretched to produce 10% strain. F_s was then used as F_{cmd} for cyclic stretching at a frequency of 1 Hz. The F_{cmd} corresponding to the four sheets was about 0.5, 1.1, 5.7, and 10.3 mN, respectively. The displacement- and force-controlled loading methods were applied to the four sheets. Under force control, the measured F_s of the four sheets basically fluctuated around F_{cmd}, as indicated by the blue curves in Fig. 3b. However, under displacement control, F_s gradually decreased in the initial phase (about 300 s) and then tended to stabilize at about 70% of the original F_s, as indicated by the red curves in Fig. 3b. The decay of F_s under displacement control showed that the viscoelastic hydrogel sheet underwent stress relaxation. The corresponding ε values of the four sheets under force control

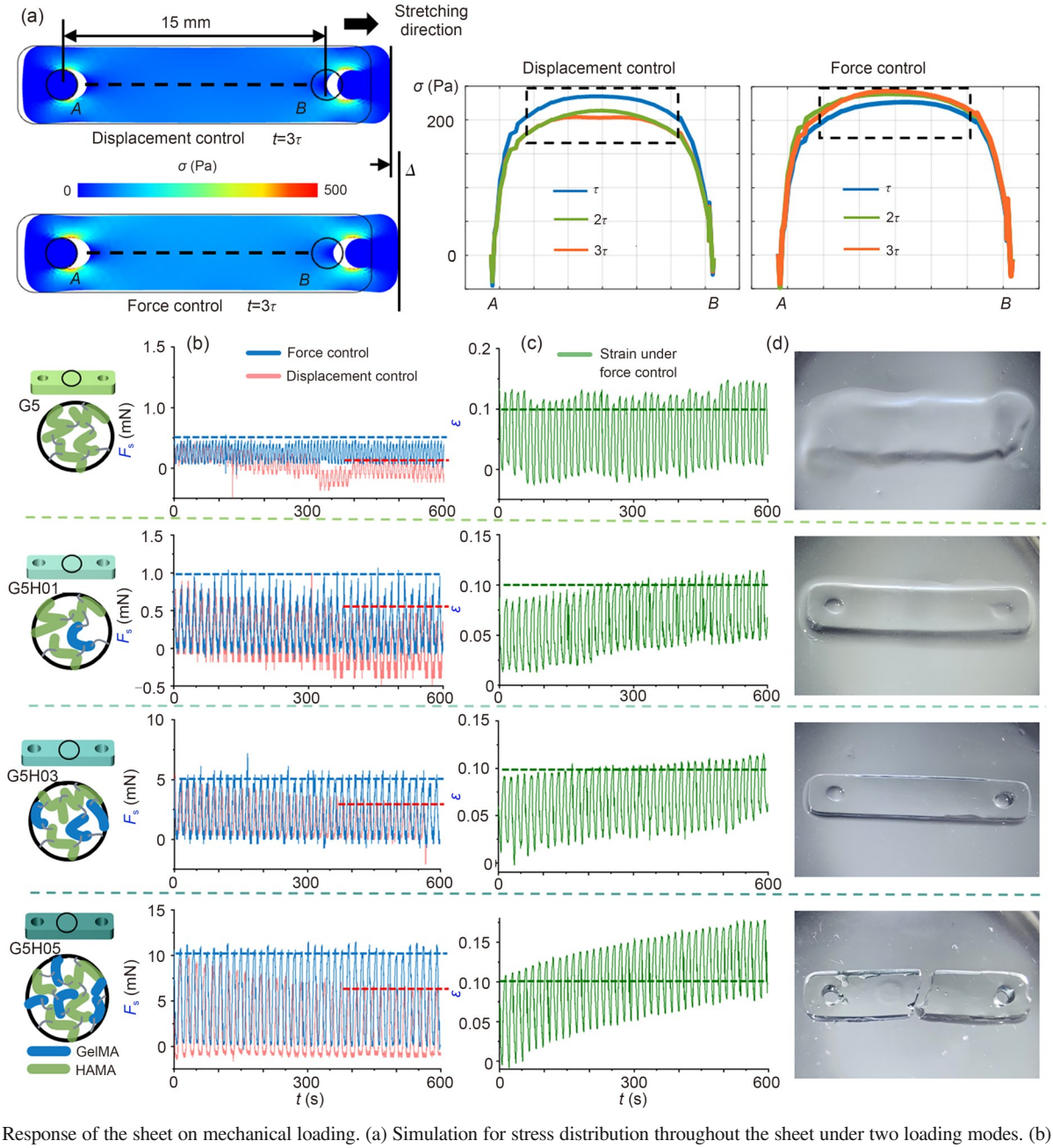

Fig. 3 Response of the sheet on mechanical loading. (a) Simulation for stress distribution throughout the sheet under two loading modes. (b) Time-dependent changes in F_s under force control and displacement control for four sheets, respectively. (c) Time-dependent changes in strain under force control for the four sheets. (d) Sheet morphology after cyclically stretching in an incubator

are shown in Fig. 3c. The initial ε of the hydrogel sheets reached approximately 10% and then continuously increased with progressive dynamic stretching. Furthermore, the composite modulus E^* in the different groups at 1 Hz can be calculated by σ and ε. The values of E^* in the four groups were 0.8, 2.0, 10.6, and 17.0 kPa, respectively. Compared with data reported in related studies [27], the measured moduli are largely consistent, indicating the accuracy of the measurement system.

When F_{cmd} was set as the original F_s under 20% and 30% amplitude strain, a similar sheet response was achieved in all four sheets. However, although an increase in the sheet creep distance was observed with increasing strain, no significant difference in the decay time of F_s was observed. After continuous mechanical stretching in the incubator for approximately 5 h, the morphology of the four sheets is shown in Fig. 3d. The sheet in G5 exhibited structural collapse due to the combined effect of swelling and low mechanical strength. When 0.1% HAMA was added, the morphology of the hydrogel remained nearly intact; however, an obvious tendency toward collapse was observed, indicating that the sheet in G5H01 had difficulty maintaining its structure for

14 d of dynamic stretching during cell culture. When the HAMA concentration was increased to 0.3%, the sheet maintained its original shape. In the cell-free state, the structure of the hydrogel sheet remained stable after force-controlled cyclical stretching for 24 h. However, when the HAMA concentration reached 0.5%, internal fracturing of the hydrogel sheet occurred after continuous mechanical loading for approximately 2 h, and the original morphology could not be maintained. Therefore, here, we chose the sheet in the G5H03 group as the vehicle for long-term force-stimulated 3D cell culture.

3.3 Response of BMSCs encapsulated in sheets to force-controlled strain application

BMSCs were encapsulated in the G5H03 hydrogel sheet. Force stimulation was then applied to the sheet using a stretching culture instrument for a long period. The F_S-induced mechanical loading schematic is shown in Fig. 4a. The first day was devoid of mechanical stimulation to establish stable adhesion between BMSCs and the inner network of the sheet. Commencing on Day 2, F_S was applied at a frequency of 1 Hz for 20 min at a 3-h interval, which was maintained throughout the remainder of the 14-d culture period. The strain of the sheet was maintained at 10% amplitude for displacement control (MD), and F_{cmd} was set as F_S under the initial strain at 10% amplitude for force control (MF). Figure 4b shows the time-dependent change in F_S under the two loading methods. For MF, F_S remained stable over the 14-d culture period. Conversely, for MD, a progressive decrease in F_S due to the effect of stress relaxation was observed. Furthermore, the BMSC-free sheet was used as a control group to evaluate the effect of cell activity on force stimulation. The trend of change in F_S of the BMSC-free sheet was consistent with that of the BMSC-laden sheet; however, the diminution of F_S in the BMSC-free sheet was less severe than that in the BMSC-laden sheet. This discrepancy is likely because of the secretion of various enzymes by BMSCs, which greatly accelerate the degradation of GelMA; thus, the mechanical properties of the sheet become too weak to generate enough deformation to maintain F_S.

To further evaluate the growth of BMSCs in the sheets, we set up three groups responding to three stimulation conditions: static culture (M0), MD, and MF. Based on the CCK-8 method, the cell proliferation rate in the three groups was quantitatively analyzed, as shown in Fig. 4c. The M0 group exhibited the lowest rate of cell proliferation, whereas increased cell proliferation was observed in the other two groups. In particular, BMSCs in the MF group exhibited more rapid proliferation than those in the MD group on Days 4 and 7. This result shows that the force-controlled loading method is a better strategy for cell growth than the displacement-controlled loading method. Subsequent live/dead staining experiments affirmed that cells maintained high viability, and the change in cell density during 7 d of cell culture further revealed that the measurement of the cell proliferation rate was accurate. The cytoskeletal staining revealed that the cells in the M0 group were sparsely distributed within the hydrogel. In contrast, mechanical stimulation resulted in a more uniform dispersion of cells, with a dendritic morphological extension and evident cellular interactions. Notably, the MF group exhibited higher cell densities than the MD group, and cellular growth exhibited a directional pattern, characterized by cytoskeletal extension aligning with the direction of mechanical stimulation (Fig. 4d). mRNA sequencing revealed a significant number of DEGs (Fig. S5a in the supplementary information), with 914 upregulated and 863 downregulated genes (Fig. S5b in the supplementary information). The clustering heat map of DEGs clearly demonstrates the distinct separation between the MF and M0 groups (Fig. S5c in the supplementary information), validating the reliability of the differential expression analysis results. GO enrichment analysis indicates that these DEGs are predominantly enriched in biological processes, such as extracellular matrix organization, extracellular structure organization, external encapsulating structure organization, and cell-substrate adhesion (Fig. 4e). KEGG enrichment analysis suggests that DEGs are primarily involved in signaling pathways, including focal adhesion, MAPK signaling pathway, and PI3K-Akt signaling pathway (Fig. 4f).

3.4 Mechanical stimulation promoting the secretion and functionalization of BMSC-exos

The BMSC-exo production process in each group is shown in Fig. 5a. The results of transmission electron microscopy (TEM) exhibited that the three groups of exosomes showed typical dish structures, and no significant differences in morphology were observed (Fig. 5b). We identified the surface markers of the extracted exosomes by Western blotting. The exosome-specific markers CD81, CD9, and TSG101 were positively expressed in the three groups of BMSC-exos; however, Calnexin was not expressed (Fig. 5c). NTA results (Fig. 5d) showed that the particle sizes of the three groups of BMSC-exos were consistent with the distribution characteristics of exosomes. These results confirmed the successful extraction of BMSC-exos. We found that mechanical stimulation could significantly increase the secretion of BMSC-exos. The secretion of BMSC-exos in the MD and MF groups was significantly higher than that in the M0 group, and the secretion of BMSC-exos in the MF group was the highest, approximately 3.3 times that in the MD group and 8.5 times that in the M0 group (Fig. 5e). From the cellular uptake experiments, red-labeled exosomes were observed around the nucleus in all three groups, indicating that all three groups of BMSC-exos could be normally taken up by BMSCs (Fig. 5f).

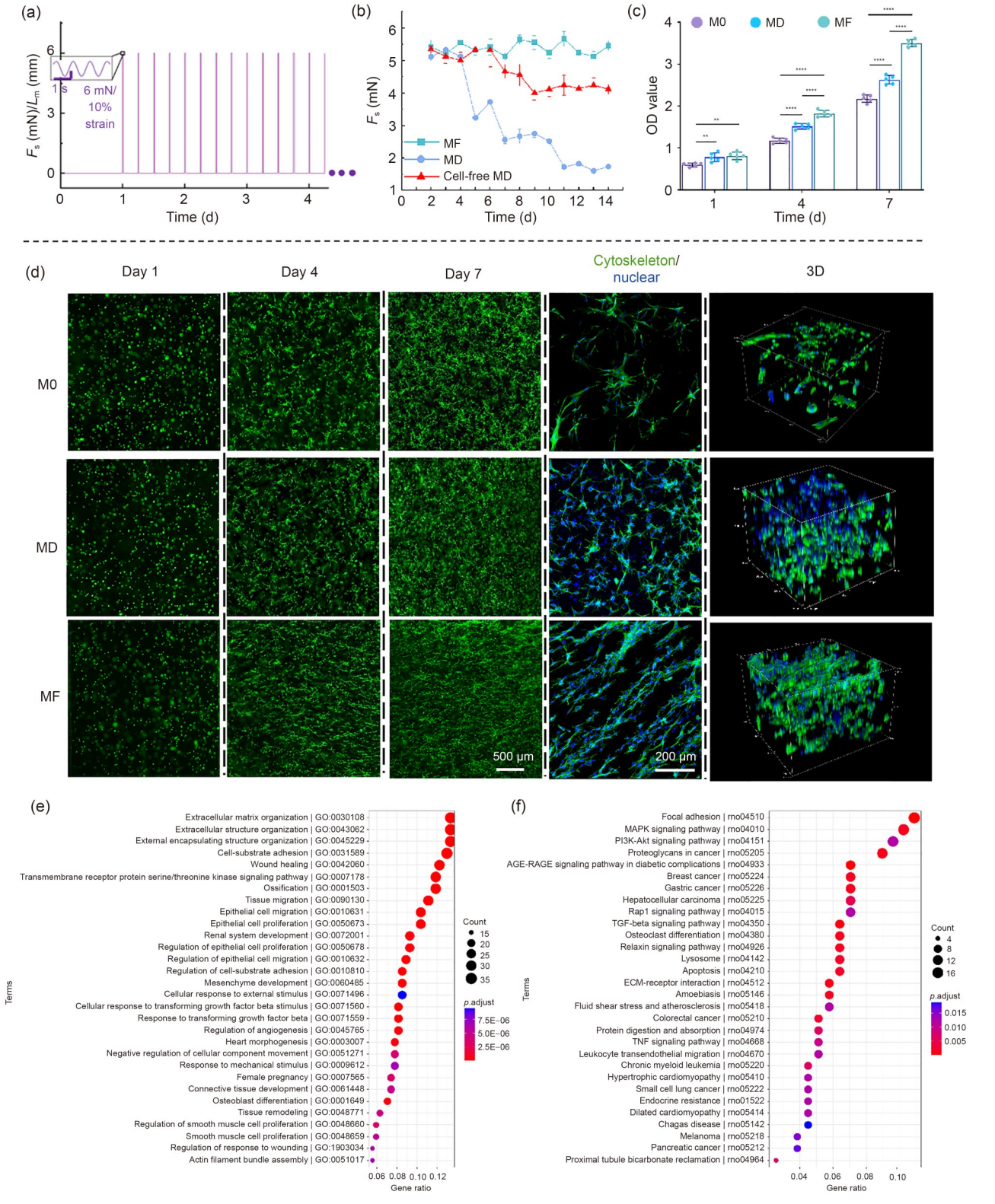

Fig. 4 Response of BMSCs encapsulated in the sheets to mechanical loading. (a) Mechanical loading strategy. (b) Time-dependent change in F_s under different loading modes. (c) Effects of three loading modes on the proliferation of the encapsulated BMSCs. Data are expressed as mean± standard deviation (n=5; $^{**}p$<0.01, $^{****}p$<0.0001). (d) Live/Dead staining of BMSCs in different mechanical loading groups (green: live cells; red: dead cells) at 1, 4, and 7 d and cytoskeleton staining (green: F-actin stained with FITC-phalloidin; blue: nucleus stained with DAPI) of BMSCs in different mechanical loading groups on the seventh day of culture. (e) GO enrichment analysis of DEGs. (f) KEGG enrichment analysis of DEGs. OD: optical density

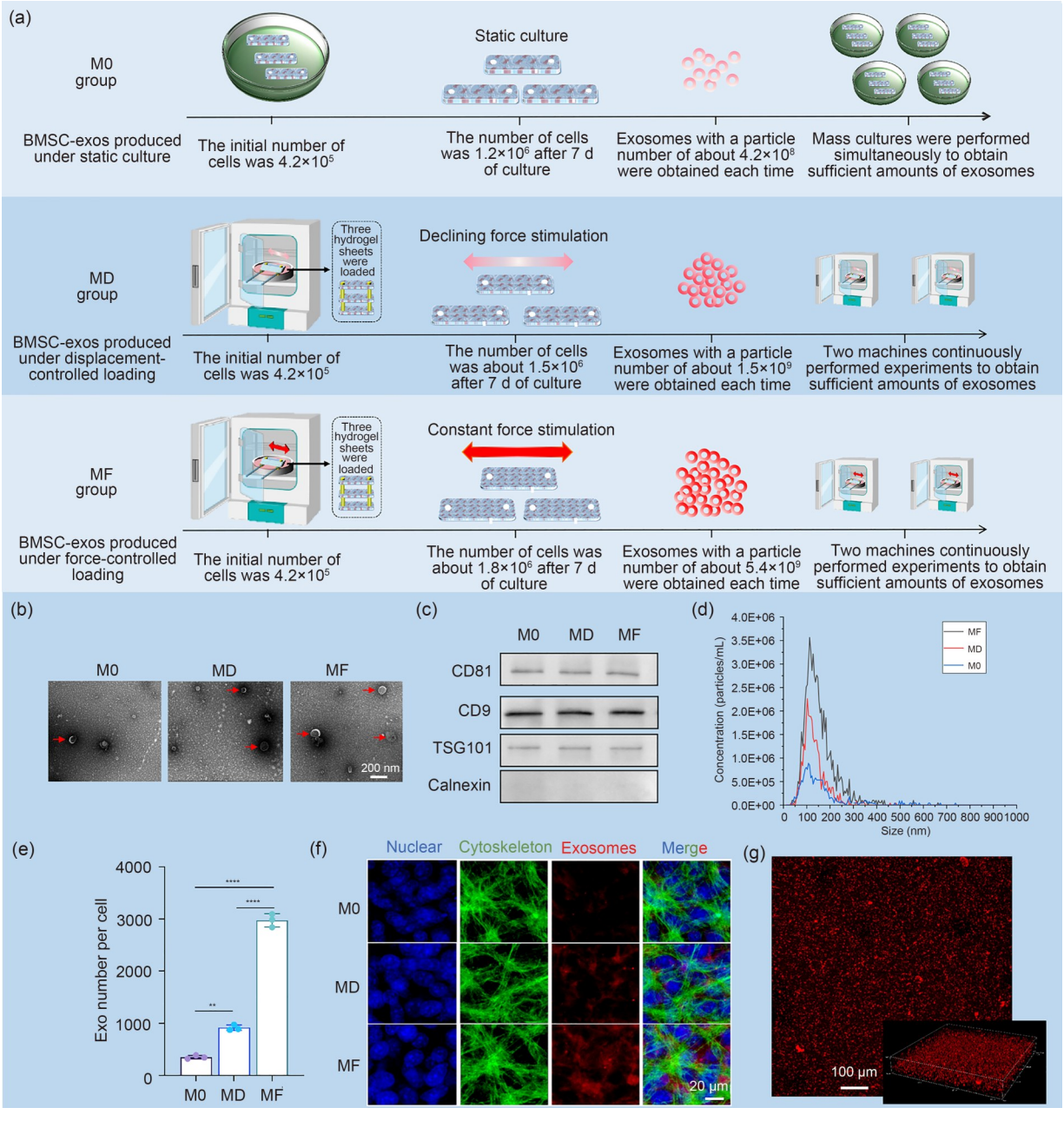

Fig. 5 Extraction and identification of BMSC-exos. (a) Schematic of BMSC-exo production in different groups. (b) TEM images of BMSC-exos secreted in the M0, MD, and MF groups. (c) The surface markers CD81, CD9, TSG101, and Calnexin of BMSCs and BMSC-exos in the M0, MD, and MF groups were identified using Western blotting. (d) Representative size distribution of BMSC-exos in the M0, MD, and MF groups. (e) Number of BMSC-exos secreted by each cell in the M0, MD, and MF groups (data are expressed as mean±standard deviation, n=3; $^{**}P<0.01$, $^{****}P<0.0001$). (f) Fluorescence images of cell uptake of BMSC-exos from the M0, MD, and MF groups. (g) Fluorescence image of exosomes uniformly distributed in the hydrogel

In the MF group, a higher number of BMSC-exos accumulated around the nucleus, suggesting that BMSC-exos produced by continuous and stable mechanical stimulation were more likely to be taken up by BMSCs. Via fluorescence microscopy, we also found that BMSC-exos could be evenly encapsulated within the hydrogel (Fig. 5g).

To evaluate whether BMSC-exos induced by mechanical stimulation have a better ability to promote osteogenic differentiation, we performed 3D co-culture of BMSCs and BMSC-exos. qRT-PCR analysis was performed to measure the expression of osteogenic genes. By the 7th day of cultivation, the expression levels of the osteogenic-related genes runt-related transcription factor 2 (*RUNX2*) (Fig. 6a), *ALP* (Fig. 6b), osteopontin (*OPN*) (Fig. 6c), and osteocalcin (*OCN*) (Fig. 6d) in the MF group were significantly higher than those in the M0 and MD groups. This trend remained

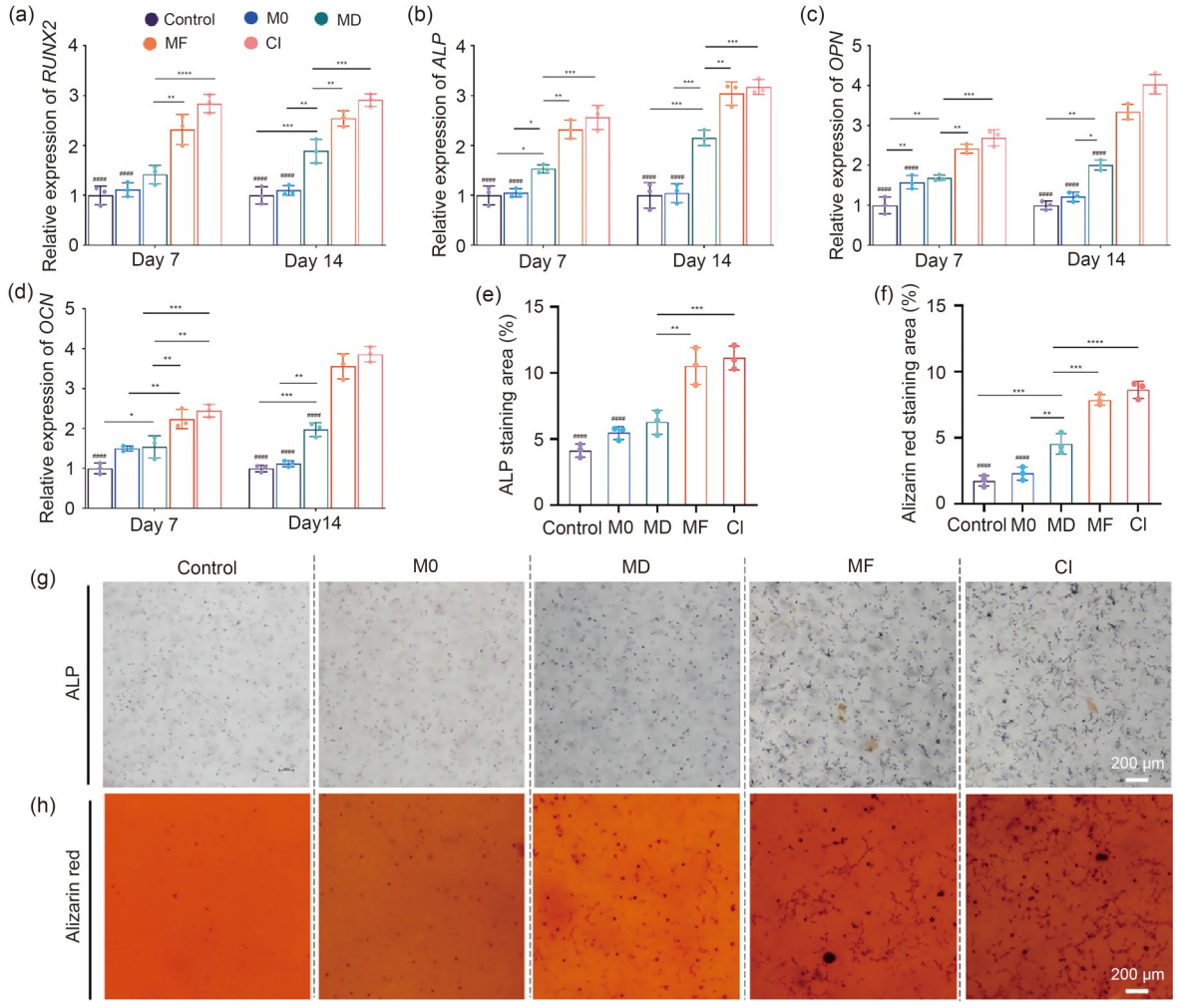

Fig. 6 Osteogenic differentiation of BMSCs induced by BMSC-exos from different treatment groups. (a–d) Expression of osteogenesis-related genes in each group after 7 and 14 d of culture. Quantitative analysis of positive areas of ALP (e) and alizarin red (f) staining. ALP (g) and alizarin red (h) staining images of BMSCs. Data are expressed as mean±standard deviation (n=3). $^{*}p$<0.05, $^{**}p$<0.01, $^{***}p$<0.001, $^{****}p$<0.0001; $^{\#\#\#\#}p$< 0.0001 compared with the MF and CI groups

on Day 14. At the two selected time points, the expression of osteogenic-related genes in the MF group was close to that in the CI group. These results suggest that the constant force stimulation applied in the MF group could promote the production of exosomes with stronger osteogenic capacity and has similar effects to chemical induction. Furthermore, we observed that the expression of osteogenic genes in the MD group was higher than that in the M0 group. However, it was still lower in the MD group than in the MF group, indicating that displacement-controlled mechanical loading could enhance the osteogenic ability of BMSC-exos, but not to the same extent as force-controlled loading.

To further investigate the osteogenic induction ability of BMSC-exos induced by mechanical stimulation, we performed ALP and alizarin red staining assays. The statistical results of ALP staining (Fig. 6e) revealed that prominent ALP-positive areas were observed in the MF and CI groups on the 7th day of culture, with no significant difference in the extent of staining between these two groups. Conversely, the M0 group displayed scarcely any ALP-positive area. The ALP-positive area in the MD group was higher than that in the M0 group but lower than that in the MF and CI groups. Furthermore, the statistical results of alizarin red staining (Fig. 6f) revealed calcium nodule deposition in the MF and CI groups on Day 14, whereas no obvious calcium nodule staining was observed in the M0 group. Some areas of calcium nodule staining could be observed in the MD group, but less so than in the MF and CI groups. Representative images of ALP and alizarin red staining are shown in Figs. 6g and 6h, respectively.

3.5 Constant force stimulation-induced BMSC-exos showing strong osteoinductivity

The constructed 5-mm bone defect was a critical bone defect in rats, which would be unlikely to self-repair without

intervention. Therefore, such a rat model was used to verify the capacity of constant force stimulation-induced BMSC-exos to repair the bone defect, as shown in Fig. 7a. Furthermore, three other groups were included: the Defect group, M0 group, and MD group. Micro-CT results obtained at the eighth postoperative week revealed that the Defect group (Fig. 7b) showed a lower bone volume fraction (Fig. 7f), trabecular thickness (Fig. 7g), and trabecular number (Fig. 7h), significantly lagging behind both the two stimulated BMSC groups. The M0 group (Fig. 7c) exhibited an improvement in bone repair indices compared with the Defect group, although the difference did not reach statistical significance. The bone repair indices in the MD group (Fig. 7d) were higher than those in the Defect and M0 groups, which may be related to the promotion of the osteogenic ability of BMSC-exos by mechanical stimulation. The MF group (Fig. 7e) outperformed all three groups in terms of bone repair indices, with statistically significant differences. Furthermore, the structural index (Fig. 7i) in the sheet in the MF group was 1.34 ± 0.13, closer to 1 than that in the other groups, suggesting that the newly formed bone tissue was more mature and closely resembled plate-like bone structure.

The osteoinductive capacity was further assessed using HE and Masson staining (Figs. 7j and 7k). The HE staining results indicated complete degradation of the hydrogel in all groups, with no residual hydrogel observed. Furthermore, no obvious inflammatory cells were observed, suggesting good biocompatibility of the hydrogel and BMSC-exos implant without inducing a significant rejection reaction. Masson staining results revealed few blue-stained areas representing new bone tissue in the Defect group, slightly more in the M0 group, a substantial amount in the MD group, and an abundance of new bone tissue and red-stained mature bone tissue repairing the bone defect area in the MF group. These findings suggest that BMSC-exos exhibit stronger osteoinductive ability under mechanical stimulation, particularly under force-controlled loading.

4 Discussion

Exosomes are extracellular vesicles released by cells, containing various bioactive molecules [28, 29]. As important signaling molecules, exosomes constitute a novel cell–cell information transmission system and participate in various biological processes including cell communication, cell migration, angiogenesis, and tumor cell regulation [30]. Most of the functions performed by BMSCs are mediated through BMSC-exos [10]. Furthermore, the use of exosomes circumvents the tumorigenicity associated with stem cell proliferation disorders and offers advantages such as facile transportability and application, direct fusion with target cells to exert biological effects, and low immunogenicity [31]. Therefore, cell-free therapy based on exosomes has emerged as a research focus and has been applied to the treatment of various diseases, such as cancer [32], orthopedic diseases [33], chronic refractory wounds [34], and nerve injury [17]. However, the engineering application of exosomes is confronted with the challenge of low yield and reduced biological activity [10]. Various chemical, physical, and environmental factors have been explored to enhance the production of exosomes. Physical inducers have received increasing attention because of their advantages over chemical inducers, including higher biosafety and lack of dose dependence [35, 36]. Among them, mechanical signaling is an important pathway for cell–cell and cell–environment communication. Therefore, regulating the secretion of exosomes by mechanical stimulation becomes possible. Hao et al. [25] developed a novel and high-throughput microfluidic device to permeabilize the cell membrane by applying mechanical squeezing stimulation, which led to an approximately four-fold increase in the secretion of extracellular vesicles. Furthermore, hydrodynamics and stretch stimulation have been shown to promote the secretion of extracellular vesicles [14, 37]. Studies on the use of mechanical stimulation to enhance exosome secretion have mainly focused on 2D culture models [12, 14, 15]. Although this method simplifies research, it significantly differs from the physiological 3D cell growth environment. These dimensional differences critically influence cellular responses to stimuli [16, 18, 38, 39]. Furthermore, 3D culture alone has been shown to enhance the secretion of exosomes, and when combined with mechanical stimulation, there is a synergistic effect that further promotes exosome secretion [40, 41]. Therefore, investigating the impact of mechanical stimulation on the secretion of exosomes in a 3D culture environment is important.

In this study, we explored a force-controlled mechanical loading method suitable for 3D culture. We explored a 3D culture system that was suitable for both BMSC growth and mechanical stimulation. Synthetic hydrogels, which can mimic the cellular microenvironment in physiological conditions, play a crucial role in studying cell responses to various physicochemical signals within 3D culture systems [42, 43]. Obtaining the ideal composite hydrogel is feasible by blending different hydrogels [44, 45]. Our findings suggest that a 3D culture system consisting of 5% GelMA and 0.3% HAMA achieves a balance between cytocompatibility and mechanical properties, which is crucial for prolonged exposure to mechanical loading [26, 46]. Among the various mechanical stimuli endured by cells, stretching stimulation has been extensively studied. In 2D cultures, stretching can be easily applied using an elastic culture plate combined with a stretching system [15, 37, 47]. However, implementing stretching stimulation in a soft hydrogel-based 3D culture system presents challenges. Liu et al. [21, 22] developed a deformable membrane platform for mechanically stretching

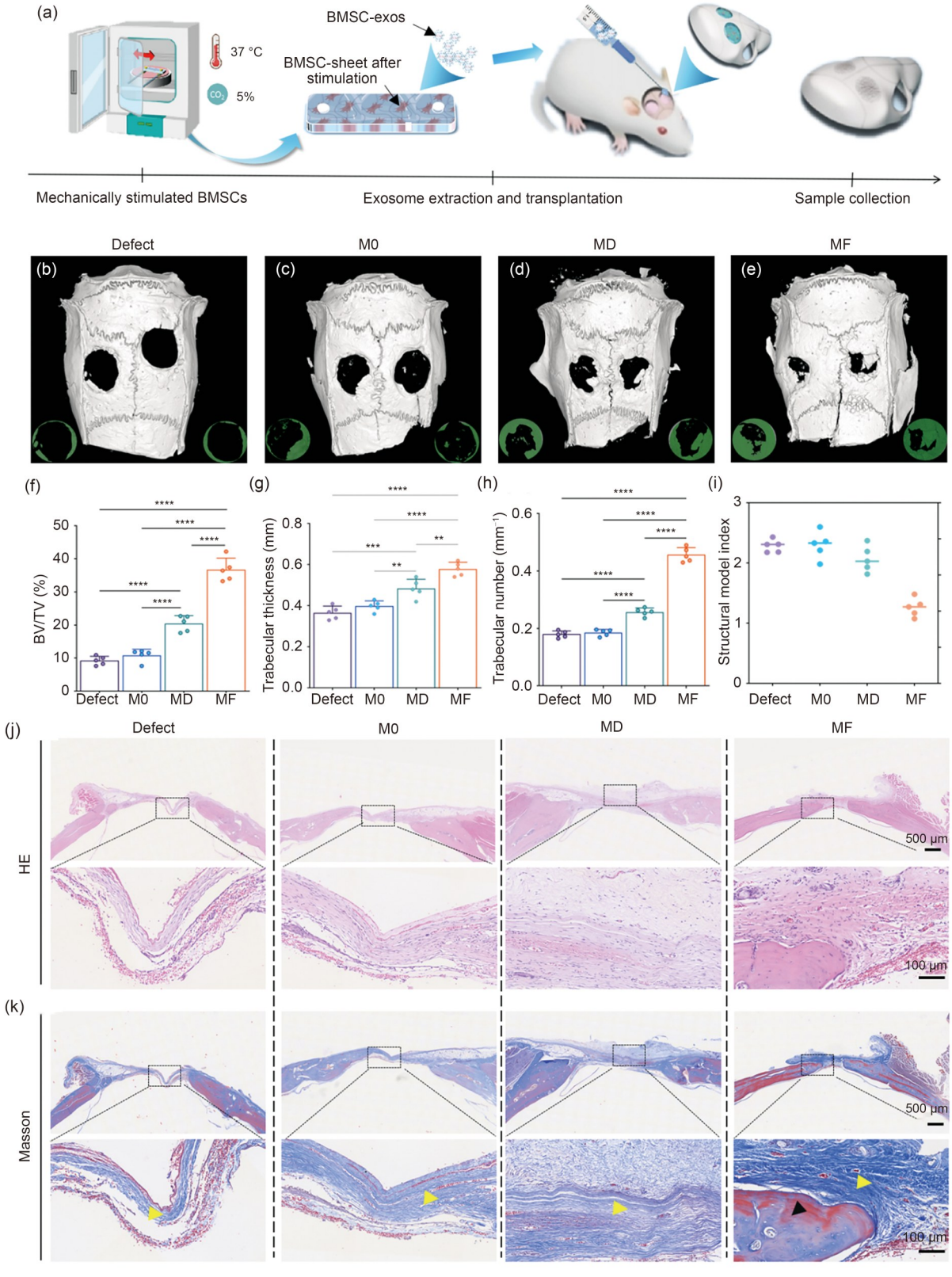

Fig. 7 Repair of bone defects based on the stimulated BMSC-exos. (a) Design of animal experiments. Micro-CT scan images of skull defects in the Defect (b), M0 (c), MD (d), and MF (e) groups (green represents newly formed bone tissue). (f–i) Micro-CT quantitative statistics of osteogenesis-related parameters for the four groups (data are expressed as mean±standard deviation, n=5; $^{**}p<0.01$, $^{***}p<0.001$, $^{****}p<0.0001$). HE (j) and Masson (k) staining of skull defects of bone regeneration at eight weeks after surgery in a rat calvarial defect model (yellow arrows indicate areas of new bone tissue; the black arrow indicates areas of mature bone tissue)

and compressively stimulating cells in a 3D culture system. However, they also observed that their method induces a complex, spatially heterogeneous 3D strain field in the hydrogel, which includes in-plane biaxial tension and through-thickness compression. Therefore, the system cannot be used to accurately control a single strain component, posing a challenge to mechanistic research. Yu et al. [20] developed a 3D culture environment based on hydrogels and applied mechanical stimulation at 20% strain to investigate the effect of mechanical stimulation on the secreted exosomes. However, the decay in hydrogel mechanical properties over time indicates that displacement-controlled loading decreases mechanical stimulation intensity. Real-time mechanical monitoring and feedback adjustments are crucial for maintaining consistent mechanical loading [48]. In this study, we used innovative mechanical loading systems along with a long hydrogel sheet-based 3D culture system to ensure spatially homogeneous stretching stimuli. The system's ability to monitor mechanical parameters in real time and perform feedback regulation ensured the consistency of mechanical stimulation during experiments.

Studies have shown that appropriate mechanical stimulation can enhance the proliferation of BMSCs [49, 50], whereas excessive mechanical stimulation can result in cell death [51]. In our study, we observed that the two stimulation methods could significantly promote cell proliferation, suggesting that the applied stimulation fell within the physiological range. The MF conditions exhibited a greater ability to promote BMSC proliferation than the MD conditions, which was attributed to the force-controlled loading mode that provided continuous and constant cell stimulation throughout the experiment. Enhanced cell proliferation is also advantageous for improving exosome production. Using the force-controlled loading system and 3D culture system that we developed, we investigated the effect of stretching stimulation on the secretion of BMSC-exos. Our findings revealed that after 7 d of mechanical stimulation, the secretion of BMSC-exos in the MD and MF groups was higher than that in the M0 group, indicating that stretch mechanical stimulation effectively promotes BMSC-exos secretion, consistent with the findings of previous studies [14, 37]. Furthermore, the secretion of exosomes in the MF group was the highest. The average exosome secretion from a single cell in the MF group was approximately 3.3 times that in the MD group and 8.5 times that in the M0 group. This finding indicates that force-controlled loading had a superior ability to stimulate BMSC-exos secretion. Sequencing and bioinformatics analysis results indicate that mechanical stimulation enhances cell–cell and cell–matrix interactions, which is consistent with previous reports [52]. Furthermore, DEGs are involved in many key pathways. Therefore, we believe that the gene-level changes induced by mechanical stimulation are crucial for promoting BMSC-exos secretion. In contrast to the gradual decay of displacement-controlled loading during the loading process, force-controlled loading can continuously activate relevant pathways, thus enhancing exosome production.

Enhancing the function of exosomes is also a research focus. Yan et al. [53] found that mechanical stimulation not only increased the production of exosomes but also enhanced their ability to repair cartilage defects. The significance of mechanical stimulation in osteogenesis is well documented, with its regulatory effects on BMSCs being extensively explored [35, 54–57]. BMSC-exos induced by cyclic mechanical stretch have been shown to inhibit osteoclast generation and mitigate bone loss caused by mechanical unloading in a hind limb unloading mouse model by inhibiting the activity of the NF-κB signaling pathway [14]. It has also been reported that a 3D culture environment can enhance the osteoinductive ability of MSC-derived exosomes [11, 20]. In this study, we further investigated the effect of mechanically stimulated BMSC-exos on the osteogenic differentiation of BMSCs. Our findings indicate that mechanical stimulation-induced BMSC-exos could better promote osteogenic differentiation. Notably, the osteogenic effect of the MF group was superior to that of the MD group, which may be attributed to the continuous and stable mechanical stimulation in the MF group. The integration of biologically active materials by loading exosomes is a crucial approach in tissue engineering [33]. Furthermore, pretreatment of cells can increase the production of active exosomes, thereby further improving the functionality of tissue engineering materials [11, 31, 58]. Our study further investigated whether mechanically loaded BMSC-exos could enhance the osteoinductive potential of bone repair materials in vivo. The results indicated that compared with nonstimulated BMSC-exos, mechanically stimulated BMSC-exos exhibited superior osteoinduction and enhanced bone repair in vivo, highlighting the importance of mechanical stimulation in BMSC tissue engineering. Furthermore, our findings suggest that force-controlled mechanical loading is a novel approach for large-scale production of functionally enhanced BMSC-exos. Note that this study represents a preliminary exploration of the promotion of BMSC-exos secretion and enhancement of their function through force-controlled loading. Further research is necessary to elucidate the relevant mechanisms.

5 Conclusions

To summarize, we used an innovative mechanical loading system specifically designed for the uniform and consistent mechanical stimulation of cells and successfully applied it to a hydrogel-based 3D culture system. Compared with displacement-controlled loading, force-controlled loading with this system demonstrated a superior ability to promote BMSC-exos secretion. Furthermore, BMSC-exos induced

by mechanical loading exhibited better osteogenic ability. The development of this mechanical stimulation system helps overcome the challenges associated with low yield and insufficient functionality in tissue engineering applications of BMSC-exos.

Supplementary Information The online version contains supplementary material available at https://doi.org/10.1631/bdm.2400231.

Acknowledgements The authors are grateful for the funding support from the National Key Research and Development Program of China (No. 2021YFB3802105-3) and the National Natural Science Foundation of China (No. 62173043).

Author contributions JW and HW contributed to conceptualization, investigation, data curation, writing—original draft, formal analysis, and visualization. TS helped in methodology, funding acquisition, and writing—review & editing. QS and XC helped in methodology and validation. YBQ and ST helped in supervision and project administration. DHL and JHZ contributed to conceptualization, methodology, funding acquisition, and writing—review & editing.

Declarations

Conflict of interest The authors declare that they have no conflict of interest.

Ethical approval All institutional and national guidelines for the care and use of laboratory animals were followed. In vivo experiments were conducted in accordance with the Chinese Animal Experimentation Law and approved by the PLA General Hospital Ethics Committee (Approval No. 2022-X18-136).

Data availability The data that support the findings of this study are available from the corresponding authors upon reasonable request.

References

1. Tovar N, Witek L, Atria P et al (2018) Form and functional repair of long bone using 3D-printed bioactive scaffolds. J Tissue Eng Regen Med 12(9):1986–1999. https://doi.org/10.1002/term.2733
2. Rosslenbroich SB, Oh CW, Kern T et al (2023) Current management of diaphyseal long bone defects: a multidisciplinary and international perspective. J Clin Med 12(19):6283. https://doi.org/10.3390/jcm12196283
3. Migliorini F, Padula GL, Torsiello E et al (2021) Strategies for large bone defect reconstruction after trauma, infections or tumour excision: a comprehensive review of the literature. Eur J Med Res 26(1):118. https://doi.org/10.1186/s40001-021-00593-9
4. Hao JX, Bai BS, Ci Z et al (2021) Large-sized bone defect repair by combining a decalcified bone matrix framework and bone regeneration units based on photo-crosslinkable osteogenic microgels. Bioact Mater 14:97–109. https://doi.org/10.1016/j.bioactmat.2021.12.013
5. Wang HH, Li XF, Lai SK et al (2023) Construction of vascularized tissue engineered bone with nHA-coated BCP bioceramics loaded with peripheral blood-derived MSC and EPC to repair large segmental femoral bone defect. ACS Appl Mater Interfaces 15(1):249–264. https://doi.org/10.1021/acsami.2c15000
6. Hoang DM, Pham PT, Bach TQ et al (2022) Stem cell-based therapy for human diseases. Signal Transduct Target Ther 7(1):272. https://doi.org/10.1038/s41392-022-01134-4
7. Sissung TM, Figg WD (2020) Stem cell clinics: risk of proliferation. Lancet Oncol 21(2):205–206. https://doi.org/10.1016/S1470-2045(19)30787-9
8. Wang YY, Wen J, Lu T et al (2024) Mesenchymal stem cell-derived extracellular vesicles in bone-related diseases: intercellular communication messengers and therapeutic engineering protagonists. Int J Nanomed 19:3233–3257. https://doi.org/10.2147/ijn.s441467
9. Wu D, Chang X, Tian JJ et al (2021) Bone mesenchymal stem cells stimulation by magnetic nanoparticles and a static magnetic field: release of exosomal miR-1260a improves osteogenesis and angiogenesis. J Nanobiotechnol 19(1):209. https://doi.org/10.1186/s12951-021-00958-6
10. Debbi L, Guo SW, Safina D et al (2022) Boosting extracellular vesicle secretion. Biotechnol Adv 59:107983. https://doi.org/10.1016/j.biotechadv.2022.107983
11. Yu WT, Li SN, Guan XC et al (2022) Higher yield and enhanced therapeutic effects of exosomes derived from MSCs in hydrogel-assisted 3D culture system for bone regeneration. Biomater Adv 133:112646. https://doi.org/10.1016/j.msec.2022.112646
12. Wang ZY, Maruyama K, Sakisaka Y et al (2019) Cyclic stretch force induces periodontal ligament cells to secrete exosomes that suppress IL-1β production through the inhibition of the NF-κB signaling pathway in macrophages. Front Immunol 10:1310. https://doi.org/10.3389/fimmu.2019.01310
13. Mullen M, Williams K, LaRocca T et al (2023) Mechanical strain drives exosome production, function, and miRNA cargo in C2C12 muscle progenitor cells. J Orthop Res 41(6):1186–1197. https://doi.org/10.1002/jor.25467
14. Xiao F, Zuo B, Tao B et al (2021) Exosomes derived from cyclic mechanical stretch-exposed bone marrow mesenchymal stem cells inhibit RANKL-induced osteoclastogenesis through the NF-κB signaling pathway. Ann Transl Med 9(9):798. https://doi.org/10.21037/atm-21-1838
15. Xue Z, Hu D, Tang H et al (2024) Mechanical force regulates the paracrine functions of ADSCs to assist skin expansion in rats. Stem Cell Res Therapy 15(1):250. https://doi.org/10.1186/s13287-024-03822-0
16. Gupta D, Grant DM, Hossain KMZ et al (2018) Role of geometrical cues in bone marrow-derived mesenchymal stem cell survival, growth and osteogenic differentiation. J Biomater Appl 32(7):906–919. https://doi.org/10.1177/0885328217745699
17. Han M, Yang HR, Lu XD et al (2022) Three-dimensional-cultured MSC-derived exosome-hydrogel hybrid microneedle array patch for spinal cord repair. Nano Lett 22(15):6391–6401. https://doi.org/10.1021/acs.nanolett.2c02259
18. Xie MJ, Zheng YT, Gao Q et al (2021) Facile 3D cell culture protocol based on photocurable hydrogels. Bio-Des Manuf 4(1):149–153. https://doi.org/10.1007/s42242-020-00096-2
19. Li YZ, Zhang J, Wang CZ et al (2023) Porous composite hydrogels with improved MSC survival for robust epithelial sealing around implants and M2 macrophage polarization. Acta Biomater 157:108–123. https://doi.org/10.1016/j.actbio.2022.11.029
20. Yu WT, Su XX, Li MX et al (2021) Three-dimensional mechanical microenvironment enhanced osteogenic activity of mesenchymal stem cells-derived exosomes. Chem Eng J 417:128040. https://doi.org/10.1016/j.cej.2020.128040
21. Liu HJ, MacQueen LA, Usprech JF et al (2018) Microdevice

arrays with strain sensors for 3D mechanical stimulation and monitoring of engineered tissues. Biomaterials 172:30–40. https://doi.org/10.1016/j.biomaterials.2018.04.041
22. Liu HJ, Usprech J, Sun Y et al (2016) A microfabricated platform with hydrogel arrays for 3D mechanical stimulation of cells. Acta Biomater 34:113–124. https://doi.org/10.1016/j.actbio.2015.11.054
23. Chen X, Sun T, Wei ZH et al (2022) A clamp-free microstretching system for evaluating the viscoelastic response of cell-laden microfibers. Biosens Bioelectron 214:114517. https://doi.org/10.1016/j.bios.2022.114517
24. Carroll SF, Buckley CT, Kelly DJ (2017) Cyclic tensile strain can play a role in directing both intramembranous and endochondral ossification of mesenchymal stem cells. Front Bioeng Biotechnol 5:73. https://doi.org/10.3389/fbioe.2017.00073
25. Hao R, Hu S, Zhang HT et al (2022) Mechanical stimulation on a microfluidic device to highly enhance small extracellular vesicle secretion of mesenchymal stem cells. Mater Today Bio 18:100527. https://doi.org/10.1016/j.mtbio.2022.100527
26. He J, Sun Y, Gao Q et al (2023) Gelatin methacryloyl hydrogel, from standardization, performance, to biomedical application. Adv Healthcare Mater 12(23):2300395. https://doi.org/10.1002/adhm.202300395
27. Wang M, Li WL, Hao J et al (2022) Molecularly cleavable bioinks facilitate high-performance digital light processing-based bioprinting of functional volumetric soft tissues. Nat Commun 13(1):3317. https://doi.org/10.1038/s41467-022-31002-2
28. Théry C, Zitvogel L, Amigorena S (2002) Exosomes: composition, biogenesis and function. Nat Rev Immunol 2(8):569–579. https://doi.org/10.1038/nri855
29. Raposo G, Stoorvogel W (2013) Extracellular vesicles: exosomes, microvesicles, and friends. J Cell Biol 200(4):373–383. https://doi.org/10.1083/jcb.201211138
30. EL Andaloussi S, Mäger I, Breakefield XO et al (2013) Extracellular vesicles: biology and emerging therapeutic opportunities. Nat Rev Drug Discov 12(5):347–357. https://doi.org/10.1038/nrd3978
31. Chen RJ, Feng TJ, Cheng S et al (2023) Evaluating the defect targeting effects and osteogenesis promoting capacity of exosomes from 2D- and 3D-cultured human adipose-derived stem cells. Nano Today 49:101789. https://doi.org/10.1016/j.nantod.2023.101789
32. Han QF, Li WJ, Hu KS et al (2022) Exosome biogenesis: machinery, regulation, and therapeutic implications in cancer. Mol Cancer 21(1):207. https://doi.org/10.1186/s12943-022-01671-0
33. Kang Y, Xu C, Meng LA et al (2022) Exosome-functionalized magnesium-organic framework-based scaffolds with osteogenic, angiogenic and anti-inflammatory properties for accelerated bone regeneration. Bioact Mater 18:26–41. https://doi.org/10.1016/j.bioactmat.2022.02.012
34. Peng H, Li HC, Zhang X et al (2023) 3D-exosomes laden multifunctional hydrogel enhances diabetic wound healing via accelerated angiogenesis. Chem Eng J 475:146238. https://doi.org/10.1016/j.cej.2023.146238
35. Hao ZW, Xu ZH, Wang X et al (2021) Biophysical stimuli as the fourth pillar of bone tissue engineering. Front Cell Dev Biol 9:790050. https://doi.org/10.3389/fcell.2021.790050
36. Halim A, Ariyanti AD, Luo Q et al (2020) Recent progress in engineering mesenchymal stem cell differentiation. Stem Cell Rev Rep 16(4):661–674. https://doi.org/10.1007/s12015-020-09979-4
37. Guo SW, Debbi L, Zohar B et al (2021) Stimulating extracellular vesicles production from engineered tissues by mechanical forces. Nano Lett 21(6):2497–2504. https://doi.org/10.1021/acs.nanolett.0c04834
38. Carter K, Lee HJ, Na KS et al (2019) Characterizing the impact of 2D and 3D culture conditions on the therapeutic effects of human mesenchymal stem cell secretome on corneal wound healing in vitro and ex vivo. Acta Biomater 99:247–257. https://doi.org/10.1016/j.actbio.2019.09.022
39. Yue MX, Liu YS, Zhang P et al (2023) Integrative analysis reveals the diverse effects of 3D stiffness upon stem cell fate. Int J Mol Sci 24(11):9311. https://doi.org/10.3390/ijms24119311
40. Cao JY, Wang B, Tang TT et al (2020) Three-dimensional culture of MSCs produces exosomes with improved yield and enhanced therapeutic efficacy for cisplatin-induced acute kidney injury. Stem Cell Res Ther 11(1):206. https://doi.org/10.1186/s13287-020-01719-2
41. Kim M, Yun HW, Park DY et al (2018) Three-dimensional spheroid culture increases exosome secretion from mesenchymal stem cells. Tissue Eng Regen Med 15(4):427–436. https://doi.org/10.1007/s13770-018-0139-5
42. Loebel C, Mauck RL, Burdick JA (2019) Local nascent protein deposition and remodelling guide mesenchymal stromal cell mechanosensing and fate in three-dimensional hydrogels. Nat Mater 18(8):883–891. https://doi.org/10.1038/s41563-019-0307-6
43. Huang GY, Li F, Zhao X et al (2017) Functional and biomimetic materials for engineering of the three-dimensional cell microenvironment. Chem Rev 117(20):12764–12850. https://doi.org/10.1021/acs.chemrev.7b00094
44. Xia HT, Zhao DD, Zhu HL et al (2018) Lyophilized scaffolds fabricated from 3D-printed photocurable natural hydrogel for cartilage regeneration. ACS Appl Mater Interfaces 10(37):31704–31715. https://doi.org/10.1021/acsami.8b10926
45. Gan SQ, Zheng Z, Zhang M et al (2023) Lyophilized platelet-rich fibrin exudate-loaded carboxymethyl chitosan/GelMA hydrogel for efficient bone defect repair. ACS Appl Mater Interfaces 15(22): 26349–26362. https://doi.org/10.1021/acsami.3c02528
46. Nedunchezian S, Wu CW, Wu SC et al (2022) Characteristic and chondrogenic differentiation analysis of hybrid hydrogels comprised of hyaluronic acid methacryloyl (HAMA), gelatin methacryloyl (GelMA), and the acrylate-functionalized nano-silica crosslinker. Polymers 14(10):2003. https://doi.org/10.3390/polym14102003
47. Charoenpanich A, Wall ME, Tucker CJ et al (2014) Cyclic tensile strain enhances osteogenesis and angiogenesis in mesenchymal stem cells from osteoporotic donors. Tissue Eng Part A 20(1–2): 67–78. https://doi.org/10.1089/ten.tea.2013.0006
48. Qin Y, Hu XB, Fan WT et al (2021) A stretchable scaffold with electrochemical sensing for 3D culture, mechanical loading, and real-time monitoring of cells. Adv Sci 8(13):e2003738. https://doi.org/10.1002/advs.202003738
49. Hao J, Zhang YL, Jing D et al (2015) Mechanobiology of mesenchymal stem cells: perspective into mechanical induction of MSC fate. Acta Biomater 20:1–9. https://doi.org/10.1016/j.actbio.2015.04.008
50. Hung CT, Racine-Avila J, Pellicore MJ et al (2022) Biophysical modulation of mesenchymal stem cell differentiation in the context of skeletal repair. Int J Mol Sci 23(7):3919. https://doi.org/10.3390/ijms23073919
51. Tan JL, Kuang W, Jin ZL et al (2009) Inhibition of NFkappaB by activated c-Jun NH2 terminal kinase 1 acts as a switch for C2C12

cell death under excessive stretch. Apoptosis 14(6):764–770. https://doi.org/10.1007/s10495-009-0345-7
52. Sun J, Chan YT, Ho KWK et al (2023) "Slow walk" mimetic tensile loading maintains human meniscus tissue resident progenitor cells homeostasis in photocrosslinked gelatin hydrogel. Bioact Mater 25:256–272. https://doi.org/10.1016/j.bioactmat.2023.01.025
53. Yan LT, Liu GJ, Wu X (2020) Exosomes derived from umbilical cord mesenchymal stem cells in mechanical environment show improved osteochondral activity via upregulation of LncRNA H19. J Orthop Translat 26:111–120. https://doi.org/10.1016/j.jot.2020.03.005
54. Raman N, Imran SAM, Ahmad Amin Noordin KB et al (2022) Mechanotransduction in mesenchymal stem cells (MSCs) differentiation: a review. Int J Mol Sci 23(9):4580. https://doi.org/10.3390/ijms23094580
55. Sun YY, Wan B, Wang RX et al (2022) Mechanical stimulation on mesenchymal stem cells and surrounding microenvironments in bone regeneration: regulations and applications. Front Cell Dev Biol 10:808303. https://doi.org/10.3389/fcell.2022.808303
56. Bandaru P, Cefaloni G, Vajhadin F et al (2020) Mechanical cues regulating proangiogenic potential of human mesenchymal stem cells through YAP-mediated mechanosensing. Small 16(25): e2001837. https://doi.org/10.1002/smll.202001837
57. Argentati C, Morena F, Tortorella I et al (2019) Insight into mechanobiology: how stem cells feel mechanical forces and orchestrate biological functions. Int J Mol Sci 20(21):5337. https://doi.org/10.3390/ijms20215337
58. Yuan XG, Sun L, Jeske R et al (2022) Engineering extracellular vesicles by three-dimensional dynamic culture of human mesenchymal stem cells. J Extracell Vesicles 11(6):e12235. https://doi.org/10.1002/jev2.12235